PHOTONICS Research

Unveiling spontaneous emission enhancement mechanisms in metal–insulator–metal nanocavities

Dipa Ghindani, Alireza R. Rashed, and Humeyra Caglayan*

Faculty of Engineering and Natural Sciences, Photonics, Tampere University, 33720 Tampere, Finland
*Corresponding author: humeyra.caglayan@tuni.fi

Received 1 October 2020; revised 7 December 2020; accepted 19 December 2020; posted 21 December 2020 (Doc. ID 411456); published 27 January 2021

Recent advances in the development of a nanocavity based on a metal–insulator–metal (MIM) structure have provided a great opportunity to enhance the performance of photonic devices. However, the underlying physics behind the emission enhancement obtained from such cavities is under debate. Here, in this work, we designed and investigated MIM nanocavities to reveal the mechanisms for the observed 260-fold photoluminescence enhancement from LDS 798 fluorescent dye. This study provides a pathway to engineer the emission properties of an emitter not only through the enhancement of the Purcell factor but mainly through enhancement of the excitation rate. Our numerical simulations support the experimentally acquired results. We believe an MIM cavity and dye-based hybrid system design based on the revealed enhancement process and structural simplicity, will provide more efficient, lithography free, and low-cost advanced nanoscale devices.

https://doi.org/10.1364/PRJ.411456

1. INTRODUCTION

Tailoring the emission property of an emitter is of great interest in terms of understanding the fundamental physics as well as the application prospects. In particular, the coherent interaction of an atom with the electromagnetic field is an ideal testbed to study many fundamental aspects of quantum mechanics [1]. From an application point of view, the enhancement of spontaneous emission (SE) is vital because it can enable highly efficient light-emitting devices, low-threshold lasers [2,3], and highly efficient single-photon sources [4,5]. The emission of an emitter can be enhanced by properly tailoring its photonic environment. The environment can enhance the emission either by (i) increasing the spontaneous emission rate (i.e., Purcell enhancement), (ii) increasing the excitation rate intensity, or (iii) modifying the radiation pattern [6–8]. Among these three factors, local excitation field intensity modifies the excitation rate, while the modification in the radiative decay channels of an emitter enhances the Purcell factor. There have been several studies reported on the SE enhancement of an emitter predominantly focusing on Purcell enhancement [9,10]. These studies mainly used a photonic crystal cavity [11,12], a waveguide, and metallic structures such as metal thin film [13], grating [14], nanoantennas [15,16], and nanoapertures [17]. In all these approaches, the photonic environment is tailored to achieve the fluorescence enhancement. An efficient modification in the photonic environment of an emitter can be achieved by integrating it into an optical cavity with a high-quality factor (Q-factor) and a low-mode profile. The photonic crystal (PC) cavity is an example of a cavity that supports high Q-factor resonance [11]. However, the minimum possible mode volume offered by the PC cavity is limited by the diffraction limit [18]. In addition, the integration of a narrowband emitter with a high Q-factor cavity resonance requires intensive nanofabrication and lacks scalability. On the other hand, plasmonic nanostructures offer a low-mode volume at the plasmon resonance frequency [19]. However, due to the metallic losses, they suffer from a low Q-factor. In addition, the integration process for plasmonics nanostructures with deposited emitters in large areas is limited by their fabrication complexity. This restricts the translation of this approach for integrated photonics.

Metal–insulator–metal (MIM) structures, which emerged in recent years as high Q-factor Fabry–Perot resonators, are highly versatile to modify the properties of an emitter [20]. The ability to confine the light into the subwavelength-sized dielectric spacer is a remarkable property of an MIM cavity that has been used to demonstrate many disruptive applications in a plethora of fields from super absorption to high-resolution spatial color filters [21–23]. Among the diverse applications, the spontaneous emission rate enhancement has recently attracted the attention of the scientific community [24,25]. The fabrication simplicity and reproducibility of MIM structures are the major advantages compared to plasmonic nanocavity and PC cavity based approaches.

Prayakarao *et al.* studied the effect of the dielectric thickness of the MIM cavities on the SE rate enhancement [24]. In their study, they showed an emission enhancement of HITC dye molecules at the nonresonant wavelength of MIM cavities. On the other hand, Nyman *et al.* reported far-field fluorescence enhancement at the resonant wavelength of an IR780 dye embedded in an MIM structure [25]. They showed that the achieved enhanced emission is attributed to both the excitation rate enhancement and the Purcell factor enhancement. However, since the Stokes shift in these studied dyes is very low, the cavity resonance wavelength of the MIM overlaps efficiently with both the absorption and emission spectra of the dye molecules. In such experimental circumstances, the participation of each phenomenon in the emission enhancement process is not clearly distinguishable. These recent studies presented MIM cavities as potential candidates for SE enhancement due to their outstanding optical properties. Nevertheless, the exact mechanisms for the enhanced SE were not revealed.

We performed systematic theoretical and experimental studies to investigate underlying mechanisms related to the observed enhanced SE rate in MIM cavities. In this work, we use a silver (Ag) based MIM cavity [Ag–polymethylmethacrylate (PMMA)–Ag] to enhance the spontaneous emission rate of LDS 798 dye molecules. We observed enhancement in the photoluminescence (PL) intensity along with a change in the fluorescent lifetime components. In the studied dye-integrated hybrid system, two main mechanisms play a role in the emission enhancement process: Purcell effect enhancement due to confinement of the electromagnetic field between the two metallic films and excitation rate enhancement due to the strong cavity mode. A simultaneous overlap of the absorption and emission spectra of LDS 798 dye molecules with the cavity resonance of the designed MIM nanocavity provides the opportunity to exploit both processes to enhance the emission of hybrid systems with the highest efficiency. We show the role of the excitation rate enhancement to achieve an intensified emission in such a design. We believe our approach to the design of dye-integrated hybrid MIM systems opens the way to realize more efficient, lithography-free, and low-cost advanced nanoscale devices.

2. RESULTS AND DISCUSSION

The schematic of the fabricated MIM cavity is shown in Fig. 1(a), where the thickness of top and bottom metallic layers is 35 and 150 nm, respectively. Ag has been used for the metal layers due to its excellent plasmonic property and low losses. We deposited Ag layers using an e-beam evaporator and confirmed each layer's thickness using a profilometer. PMMA was spincoated as a dielectric layer and the thickness of the dielectric layer was varied to tune the cavity resonance. The thickness of the dielectric layer was optimized using numerical simulation (Lumerical FDTD Solutions) based on finite-difference time-domain (FDTD) method. In simulations, the periodic boundary conditions were applied in the x axis and y axis while PML (perfectly matched layer) was used in z axis. A plane wave was launched in the z axis to excite the resonance modes. The simulated reflection results for different thicknesses of the dielectric (PMMA) layers are shown in

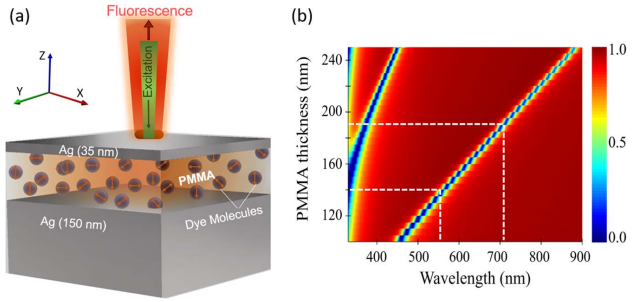

Fig. 1. (a) Schematic of MIM (Ag–PMMA + LDS 798 dye–Ag) cavity. (b) Simulated reflection result for different thicknesses of dielectric layer. White dashed lines show resonance position of both cavities with thicknesses of 140 nm and 190 nm.

Fig. 1(b). Based on these results, 140 nm and 190 nm, which correspond to the cavity resonance wavelengths of 567 and 710 nm, were chosen as the dielectric layer thicknesses to match the MIM cavity resonance with the absorption and emission spectra of LDS 798 dye molecules. We call the MIMs with PMMA thicknesses 140 nm and 190 nm MIM-I and MIM-II, respectively, in the rest of this paper. Another resonance that is blue-shifted with respect to the main resonance of the nanocavity is evident in these simulation results.

Figures 2(a) and 2(b) show the experimentally recorded absorption (black solid line) and emission spectra (red solid line) of the LDS 798 dye molecules, which confirms the absorption and emission peaks at 567 nm and 670 nm, respectively. The experimentally recorded reflection spectra for MIM-I and MIM-II are shown in Fig. 2 (blue solid line) and have good agreement with simulated reflectance results [Fig. 1(b)]. From Figs. 2(a) and 2(b), it is important to note that the resonance of the MIM-I cavity has a strong overlap with the absorption spectrum, whereas the resonance of the MIM-II cavity overlaps with the emission spectrum of the dye, but barely overlaps with the absorption spectrum.

To elucidate the effect of strong field confinement on the emission property of LDS 798, we experimentally recorded the intensity counts of the fluorescent dye molecules using PL measurement with a 532 nm excitation source. Figures 3(a) and 3(b) show PL counts for the dye integrated with MIM-I and MIM-II, respectively. From Fig. 3(a), it is evident that the incorporation of the dye molecules with the MIM-I cavity exhibits remarkable emission enhancement. We observed a 260-fold emission enhancement for the dye molecules integrated with MIM-I and only a 3-fold emission enhancement for MIM-II. In the case of MIM-I, the higher multifold enhancement can be attributed to an unequal combination of the Purcell effect enhancement and enhancement of the local excitation field, because the resonance band of the MIM-I structure overlaps strongly with the absorption spectrum and partially with the emission spectrum of the LDS 798 dye molecules. On the other hand, for MIM-II, excitation rate enhancement and Purcell factor enhancement work as two weak gateways to modify the spontaneous emission rate of the hybrid system.

Furthermore, the transient PL decay traces of the dye molecules were measured through time-resolved fluorescence

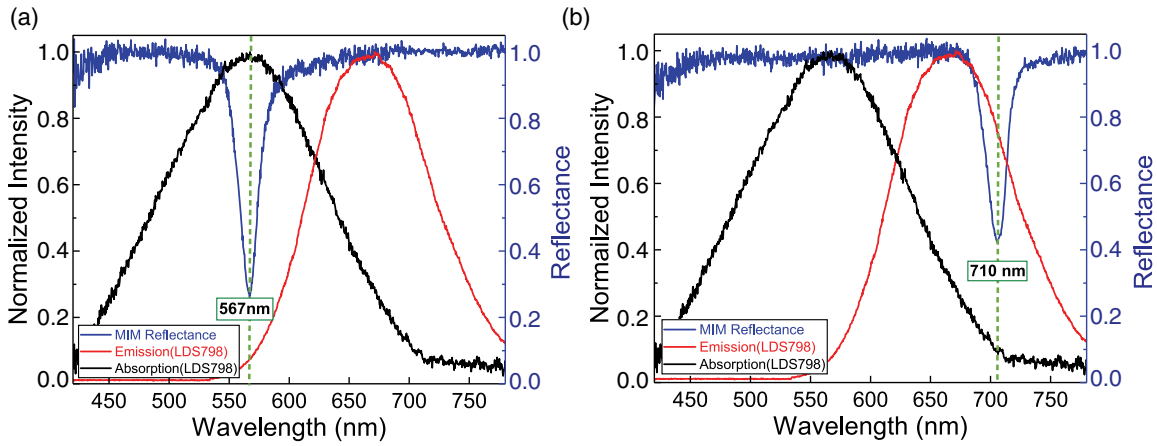

Fig. 2. Measured reflectance spectra of (a) MIM-I and (b) MIM-II cavities. The absorption and emission spectra of LDS 798 dye molecules are presented as black and red curves in both panels, respectively. The reflectance band of MIM-I cavity overlaps with the absorption peak and the emission tail of fluorescent dye, while the reflectance band of MIM-II overlaps with the emission of the dye and barely with absorption of dye.

spectroscopy. The experimentally recorded transient decay dynamics is shown in Figs. 3(c) and 3(d). We have acquired the PL lifetime of the LDS 798 dye integrated with MIM cavities I and II, and embedded them in PMMA as a reference sample. We have used a bi-exponential function to fit kinetics of the reference and main samples, as shown in Table 1. The presence of LDS 798 molecules in a rigid matrix like PMMA hinders the large-amplitude motion and intermolecular beatings of the excited molecules. Moreover, in such a dense environment, the probability of the aggregation for the monomers of the dye increases. These effects can result in two fluorescent lifetime components rather than a single component, which is the case for the dissolved LDS dye molecules in low viscous solvents [26,27]. The applied bi-exponential function to fit PL kinetics of dye molecules in the reference sample (black circles) results in two characteristic lifetime components of $\tau_1 \approx 1.144 \pm 0.009$ ns and $\tau_2 \approx 2.408 \pm 0.009$ ns, where the first component characterizes the fast decay rate, while the latter represents the slow decay process. The incorporation of the dye molecule with the MIM-I cavity induces a reduction in the fast decay component ($\tau_1 \approx 1.074 \pm 0.002$ ns), but the slow decay component ($\tau_2 \approx 3.691 \pm 0.016$ ns) gets elongated, as shown in Fig. 3(c) (red triangles).

Table 1. Time-Resolved Fluorescence Spectroscopy Results for the MIM-I and MIM-II Nanocavities and LDS 798 Dye Molecules Embedded in PMMA[a]

Sample Lable	τ_{Short} (ns)	A_{Short}	τ_{Long} (ns)	A_{Long}
LDS 798	1.144	41%	2.408	59%
MIM-I	1.074	75%	3.691	25%
MIM-II	0.990	33%	2.404	67%

[a]A bi-exponential function is used to fit kinetics of the reference and main samples. A_{Short} and A_{Long} are the amplitudes of the τ_{Short} and τ_{Long} components in percentage, respectively.

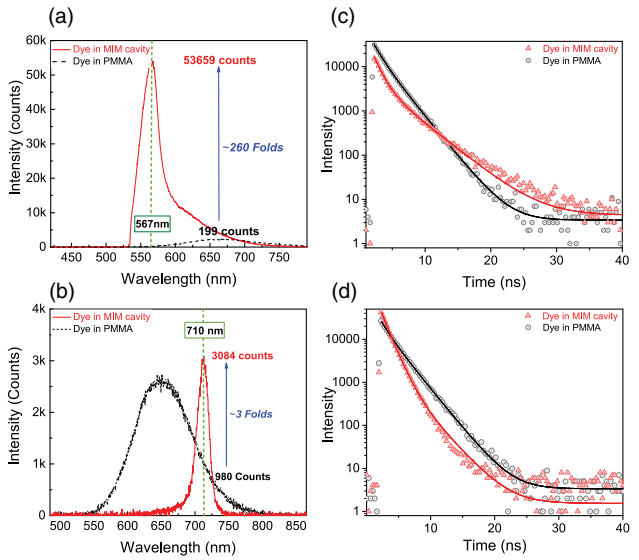

Fig. 3. Experimentally recorded steady-state PL spectra of LDS 798 dye molecules embedded in cavities (red solid lines): (a) MIM-I cavity and (b) MIM-II cavity. The recorded emission of embedded dye molecules in PMMA as a reference sample is shown as a black dotted line. Time-resolved fluorescence spectroscopy results of embedded dye molecules in the MIM cavities (red triangles): (c) MIM-I and (d) MIM-II. The recorded fluorescent lifetime of embedded dye in PMMA as a reference sample is shown as a black dotted line.

The reduction in the fast decay component can be attributed to the emission rate enhancement due to the Purcell effect. However, the slower component increases due to leakage radiation from the MIM-I cavity. Since the cavity resonance of MIM-I (at 567 nm) is far from the emission peak [670 nm, Fig. 2(a) red solid line], the part of the emission that does not couple with the MIM-I cavity results in slow leakage field. This leakage occurs due to the thin metallic top layer (35 nm), which is unable to effectively confine the emission of the nonresonant dye molecules embedded inside the cavity in the off-resonant spectral region. In the case of MIM-II, the characteristic lifetime components are $\tau_1 \approx 0.99 \pm 0.013$ ns and $\tau_2 \approx 2.404 \pm 0.009$ ns. The reduction in τ_1 arises due to the Purcell factor enhancement as the emitted radiation of

dye molecules resonantly couples with the MIM-II cavity. On the other hand, the τ_2 decay component remains almost unchanged, which depicts nonresonant emission from uncoupled dye molecules. Comparison of the fast components of the excited dye molecules in both cavities reveals an almost similar coupling strength. This happens even though the spectral overlaps between the emission of the dye molecules and the resonance bands of the two nanocavities are not similar. These results prove the occurrence of the Purcell enhancement in the MIM-I and MIM-II cavities, which leads to a similar intensified emission for both of the nanocavities through this enhancement gateway. Therefore, the excitation rate enhancement as an extra emission enhancement channel works as the main gateway to achieve a much more intensified emission only in the MIM-I cavity.

Consider that the absorption of the metallic layers can influence the emission enhancement process of the excited dye molecules. Moreover, the occurrence of nonradiative quenching mechanisms such as nanosurface energy transfer (NSET) [28] and resonance energy transfer (RET) [29] between the dye molecules and probable roughness of the metallic films is possible. In addition, the resonance energy transfer between the monomers and multimers of the dye molecules is probable [30]. However, as the time-resolved fluorescence spectroscopy results for both nanocavities do not depict extremely short lifetime components, nonradiative loss channels evidently are not influential in the emission enhancement process. This is due to the fact that the evaporated metal layers are smooth enough and a small portion of the excited dye molecules are located in the vicinity of the metallic films. Therefore, in our case, the influence of the loss mechanisms on the spontaneous decay rate enhancement is negligible.

To unveil the underlying physics for multifold enhancement, we performed numerical simulations to calculate the electric field confined inside nanocavities. Figures 4(a) and 4(b) show the electric field contour plot of MIM nanocavities with a strong electric field confinement in the dielectric region (PMMA) at cavity resonance wavelengths; i.e., 567 nm and 710 nm, respectively. Thus, one can expect that the incorporation of dye molecules with the designed MIM cavities can lead to fluorescence enhancement.

In this study, the resonance of the MIM-I cavity overlaps partially with emission spectrum while efficiently with the absorption band of the dye, as shown in Fig. 2(a), that results in an increase in fluorescence emission via two gateways: mainly by enhancing the local field intensity, which leads to a stronger population of the excited state, and slightly by increasing the spontaneous emission rate of emitter (i.e., the Purcell enhancement). Further, to emphasize our reasoning, we numerically calculated the Purcell factor of our integrated devices, as shown in Figs. 4(c) and 4(d) for the MIM-I and MIM-II cavities, respectively. For the Purcell factor calculations, we used Lumerical FDTD Solutions software, where a dipole source is used to emulate the photoexcited dye molecule. The dipole source is located in the middle of the dielectric layer of the MIM structure. The orientation of the dipole is varied from the x to y direction and the Purcell factor is averaged to capture the ensemble feature of the dye molecules that are randomly

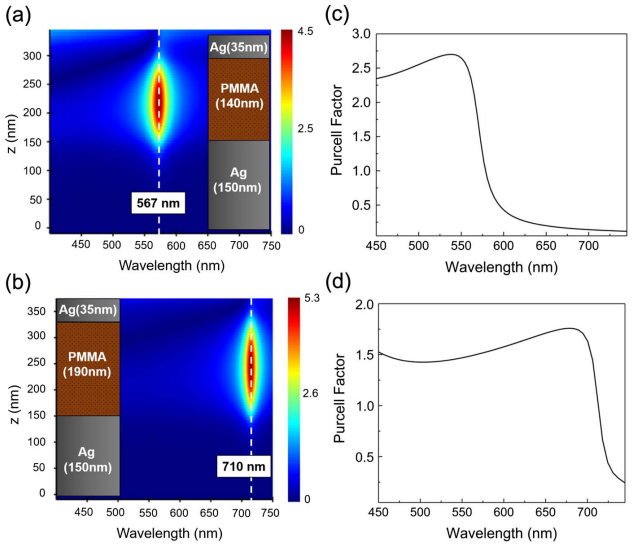

Fig. 4. Simulation results for the electric field contour plot in the two nanocavities: (a) MIM-I and (b) MIM-II. The insets in panels (a) and (b) show the schematics of the MIM-I and MIM-II designs, respectively. The Purcell factor calculation for the two cavities: (c) MIM-I and (d) MIM-II. The higher mode profile describes the lower Purcell factor of the MIM-II cavity with respect to that of MIM-I.

oriented in the x–y plane. The calculated Purcell factor for MIM-I is higher than that of MIM-II. This can be explained based on the lower mode profile of MIM-I compared to MIM-II, due to the thinner dielectric layer. As the leakage occurs in the off-resonant spectral region (above 580 nm), the observed leakage cannot influence the calculated Purcell factor for the on-resonance spectral region (540–580 nm) of the MIM-I cavity. The simulation result in Fig. 4(c) shows that, at the resonance wavelength, the Purcell factor has a value of 1.8. Such a small value of Purcell factor supports the fact that for MIM-I, the major contribution for the 260-fold enhancement is mainly coming from the excitation rate enhancement. The calculated Purcell factor for the MIM-II cavity is 1.2. This proves that, for this cavity, the contribution of the excitation rate enhancement in the acquired enhanced emission is not considerable. According to the presented approach in previous works [31,32], one can obtain the Purcell factor of a quantum emitter located inside a resonator by dividing the uncoupled emitters' lifetime by that of the coupled emitter in the cavity. Subsequently, we extracted the Purcell factor from measured lifetime results for the MIM-I and MIM-II cavities as 1.2 and 1.1, respectively. These results show adequate agreement with the calculated Purcell factors.

3. CONCLUSION

In conclusion, we have shown a fluorescence enhancement of LDS 798 dye molecules by integrating them with an MIM cavity. We unrevealed the mechanisms behind the emission enhancement process in the MIM nanocavities integrated with quantum emitters. This is performed by designing two different MIM cavities. The absorption spectrum of the dye overlaps

efficiently with the resonance of MIM-I, but barely with the resonance of MIM-II. Our comprehensive study shows that the dye integrated with MIM-II shows only a 3-fold enhancement. On the other hand, the MIM cavity that is optimized to have a resonance peak overlapping with the absorption of the dye exhibits an exceptionally high enhancement of 260-fold in the photoluminescence intensity. This arises as a combination of the Purcell effect and the excitation rate enhancement. Hence, according to our findings, the observed remarkable high emission enhancement for quantum emitters embedded in MIM nanocavities is attributed mainly to the excitation rate enhancement rather than the Purcell enhancement.

The MIM-nanocavity-based approach can be used to engineer the emission properties of an emitter by using enhanced light–matter interactions that would potentially lead to the development of efficient light-emitting devices or an enhanced energy transfer. Because MIM nanocavities possess multiple cavity modes with a high quality factor, this creates an opportunity to overlap the absorption band of a quantum emitter with the mode at the lower wavelength of the spectrum, while the emission spectrum can be overlapped with the mode at the higher wavelength. As a result, one can achieve a higher spontaneous emission enhancement for the incorporated quantum emitter inside the nanocavity. Another approach might be to integrate the dye molecule with an MIM with metasurfaces. In this way, it is possible to develop highly efficient, multifunctional integrated photonic devices where emission properties can be actively or passively tuned by changing the polarization of incident light and geometrical parameters of the metasurface. Thus, we believe our findings allow the design of low-cost, effective nanophotonic devices with enhanced functionalities.

Funding. Academy of Finland (320165 Flagship Programme PREIN).

Acknowledgment. The authors acknowledge the support of the Academy of Finland's Flagship Programme (PREIN) and The Finnish National Agency for Education through an EDUFI Fellowship for author Dipa Ghindani. The authors also thank Jussi Toppari and Gerit Groenhof for scientific discussions of the results.

Disclosures. The authors declare no conflicts of interest.

REFERENCES

1. H. Walther, B. T. H. Varcoe, B.-G. Englert, and T. Becker, "Cavity quantum electrodynamics," Rep. Prog. Phys. **69**, 1325–1382 (2006).
2. M. A. Noginov, G. Zhu, A. M. Belgrave, R. Bakker, V. M. Shalaev, E. E. Narimanov, S. Stout, E. Herz, T. Suteewong, and U. Wiesner, "Demonstration of a spaser-based nanolaser," Nature **460**, 1110–1112 (2009).
3. Q. Zhang, G. Li, X. Liu, F. Qian, Y. Li, T. C. Sum, C. M. Lieber, and Q. Xiong, "A room temperature low-threshold ultraviolet plasmonic nanolaser," Nat. Commun. **5**, 4953 (2014).
4. A. Jeantet, Y. Chassagneux, C. Raynaud, P. Roussignol, J. S. Lauret, B. Besga, J. Estève, J. Reichel, and C. Voisin, "Widely tunable single-photon source from a carbon nanotube in the Purcell regime," Phys. Rev. Lett. **116**, 247402 (2016).
5. J. Claudon, J. Bleuse, N. S. Malik, M. Bazin, P. Jaffrennou, N. Gregersen, C. Sauvan, P. Lalanne, and J.-M. Gérard, "A highly efficient single-photon source based on a quantum dot in a photonic nanowire," Nat. Photonics **4**, 174–177 (2010).
6. W. L. Barnes, "Fluorescence near interfaces: the role of photonic mode density," J. Mod. Opt. **45**, 661–699 (1998).
7. J. R. Lakowicz, "Radiative decay engineering 5: metal-enhanced fluorescence and plasmon emission," Anal. Biochem. **337**, 171–194 (2005).
8. E. Fort and S. Grésillon, "Surface enhanced fluorescence," J. Phys. D **41**, 013001 (2007).
9. A. Neogi, C.-W. Lee, H. O. Everitt, T. Kuroda, A. Tackeuchi, and E. Yablonovitch, "Enhancement of spontaneous recombination rate in a quantum well by resonant surface plasmon coupling," Phys. Rev. B **66**, 153305 (2002).
10. K. Okamoto, I. Niki, A. Shvartser, Y. Narukawa, T. Mukai, and A. Scherer, "Surface-plasmon-enhanced light emitters based on InGaN quantum wells," Nat. Mater. **3**, 601–605 (2004).
11. S. Ogawa, M. Imada, S. Yoshimoto, M. Okano, and S. Noda, "Control of light emission by 3D photonic crystals," Science **305**, 227–229 (2004).
12. K. Aoki, D. Guimard, M. Nishioka, M. Nomura, S. Iwamoto, and Y. Arakawa, "Coupling of quantum-dot light emission with a three-dimensional photonic-crystal nanocavity," Nat. Photonics **2**, 688–692 (2008).
13. Y.-J. Hung, I. I. Smolyaninov, C. C. Davis, and H.-C. Wu, "Fluorescence enhancement by surface gratings," Opt. Express **14**, 10825–10830 (2006).
14. Y. Liu and S. Blair, "Fluorescence enhancement from an array of subwavelength metal apertures," Opt. Lett. **28**, 507–509 (2003).
15. S. Kühn, U. Håkanson, L. Rogobete, and V. Sandoghdar, "Enhancement of single-molecule fluorescence using a gold nanoparticle as an optical nanoantenna," Phys. Rev. Lett. **97**, 017402 (2006).
16. O. G. Tovmachenko, C. Graf, D. J. van den Heuvel, A. van Blaaderen, and H. C. Gerritsen, "Fluorescence enhancement by metal-core/silica-shell nanoparticles," Adv. Mater. **18**, 91–95 (2006).
17. H. Rigneault, J. Capoulade, J. Dintinger, J. Wenger, N. Bonod, E. Popov, T. W. Ebbesen, and P.-F. Lenne, "Enhancement of single-molecule fluorescence detection in subwavelength apertures," Phys. Rev. Lett. **95**, 117401 (2005).
18. M. Pelton, "Modified spontaneous emission in nanophotonic structures," Nat. Photonics **9**, 427–435 (2015).
19. N. J. Halas, S. Lal, W.-S. Chang, S. Link, and P. Nordlander, "Plasmons in strongly coupled metallic nanostructures," Chem. Rev. **111**, 3913–3961 (2011).
20. Y. Kurokawa and H. T. Miyazaki, "Metal-insulator-metal plasmon nanocavities: analysis of optical properties," Phys. Rev. B **75**, 035411 (2007).
21. F. Ding, L. Mo, J. Zhu, and S. He, "Lithography-free, broadband, omnidirectional, and polarization-insensitive thin optical absorber," Appl. Phys. Lett. **106**, 061108 (2015).
22. Z. Li, S. Butun, and K. Aydin, "Large-area, lithography-free super absorbers and color filters at visible frequencies using ultrathin metallic films," ACS Photon. **2**, 183–188 (2015).
23. A. Ghobadi, H. Hajian, A. R. Rashed, B. Butun, and E. Ozbay, "Tuning the metal filling fraction in metal-insulator-metal ultra-broadband perfect absorbers to maximize the absorption bandwidth," Photon. Res. **6**, 168–176 (2018).
24. S. Prayakarao, D. Miller, D. Courtwright, C. E. Bonner, and M. A. Noginov, "Non-resonant enhancement of spontaneous emission of HITC dye in metal-insulator-metal waveguides," J. Opt. Soc. Am. B **36**, 2312–2316 (2019).
25. M. Nyman, A. Shevchenko, I. Shavrin, Y. Ando, K. Lindfors, and M. Kaivola, "Large-area enhancement of far-field fluorescence intensity using planar nanostructures," APL Photon. **4**, 076101 (2019).
26. A. R. Rashed, M. Habib, N. Das, E. Ozbay, and H. Caglayan, "Plasmon-modulated photoluminescence enhancement in hybrid plasmonic nano-antennas," New J. Phys. **22**, 093033 (2020).
27. R. Fan, Y. Xia, and D. Chen, "Solid state dye lasers based on LDS 698 doped in modified polymethyl methacrylate," Opt. Express **16**, 9804–9810 (2008).
28. C. S. Yun, A. Javier, T. Jennings, M. Fisher, S. Hira, S. Peterson, B. Hopkins, N. O. Reich, and G. F. Strouse, "Nanometal surface energy transfer in optical rulers, breaking the FRET barrier," J. Am. Chem. Soc. **127**, 3115–3119 (2005).

29. G.-C. Li, Q. Zhang, S. A. Maier, and D. Lei, "Plasmonic particle-on-film nanocavities: a versatile platform for plasmon-enhanced spectroscopy and photochemistry," Nanophotonics **7**, 1865–1889 (2018).
30. A. B. Serrano-Montes, J. Langer, M. Henriksen-Lacey, D. Jimenez de Aberasturi, D. M. Solís, J. M. Taboada, F. Obelleiro, K. Sentosun, S. Bals, A. Bekdemir, F. Stellacci, and L. M. Liz-Marzán, "Gold nanostar-coated polystyrene beads as multifunctional nanoprobes for SERS bioimaging," J. Phys. Chem. C **120**, 20860–20868 (2016).
31. T. B. Hoang, G. M. Akselrod, C. Argyropoulos, J. Huang, D. R. Smith, and M. H. Mikkelsen, "Ultrafast spontaneous emission source using plasmonic nanoantennas," Nat. Commun. **6**, 7788 (2015).
32. K. L. Tsakmakidis, R. W. Boyd, E. Yablonovitch, and X. Zhang, "Large spontaneous-emission enhancements in metallic nanostructures: towards LEDs faster than lasers," Opt. Express **24**, 17916–17927 (2016).